Available online at www.sciencedirect.com
SCIENCE DIRECT®
Journal of Molecular Catalysis A: Chemical 219 (2004) 327–342
JOURNAL OF MOLECULAR CATALYSIS A: CHEMICAL
www.elsevier.com/locate/molcata

Synthesis and characterization of soluble alkali metal, alkaline earth metal and related Keggin-type $[PMo_{12}O_{40}]^{3-}$ salts for heterogeneous catalysis reactions

Enny Silviani, Robert C. Burns*

School of Environmental and Life Sciences, Advanced Synthetic Materials Group, Chemistry Building, The University of Newcastle, Callaghan, NSW 2308, Australia

Received 6 December 2003; received in revised form 7 February 2004; accepted 15 May 2004

Abstract

Soluble $[PMo_{12}O_{40}]^{3-}$ salts of the Group 1 (Li^+ and Na^+), Group 2 (Mg^{2+}, Ca^{2+}, Sr^{2+} and Ba^{2+}) and Group 13 (Al^{3+}) metals have been synthesized and thoroughly characterized by chemical analysis, TGA/DTA, IR spectroscopy, X-ray powder diffraction (XRD), and by both solid-state and solution ^{31}P NMR spectroscopy. The structure of $Ba_3[PMo_{12}O_{40}]_2{\cdot}(55.3)D_2O$ at 150 K has also been determined by neutron powder diffraction. The compounds may be prepared by combination of $H_3[PMo_{12}O_{40}]$ and the carbonates or hydroxide/carbonates in the appropriate stoichiometry or, in the case of Al^{3+}, by addition of $Al_2(SO_4)_3$ and subsequent removal of the SO_4^{2-} as insoluble $BaSO_4$ through the addition of $BaCO_3$. All soluble $(M^{n+})_{3/n}[PMo_{12}O_{40}]$ compounds, where M^{n+} is a cation of a Group 1, 2 or 13 element, crystallize from solution with about 27–31 water molecules per $[PMo_{12}O_{40}]^{3-}$ ion. The crystallized solids are cubic (all with $a \approx 23.3$ Å), space group *Fd3m*, and are isostructural with $H_3[PMo_{12}O_{40}]{\cdot}(29–30)H_2O$. Neutron and X-ray powder diffraction show that the cations and water molecules of crystallization are effectively disordered in the interanionic voids (channels) in the unit cell, and cannot be located. There is no evidence for any co-crystallization of hydrolysed species, based on examination of the crystallized solids by IR spectroscopy and both solid-state and solution ^{31}P NMR spectroscopy.

Keywords: Phosphopolyoxomolybdate; Oxometalate; Keggin structure; Heterogeneous catalysis; Neutron diffraction

1. Introduction

Heteropolyoxometalate acids and salts are known to be highly effective heterogeneous catalysts for the gas-phase selective oxidation of organic substrates, such as aldehydes and carboxylic acids. Examples include the oxidation of methacrolein, and the oxidative dehydrogenation of isobutyraldehyde or isobutyric acid [1–7]. Oxidative dehydrogenation of isobutyraldehyde yields (primarily) methacrolein, while the other two reactions give methacrylic acid. The latter may be reacted with methanol to give methyl methacrylate, an important acrylic monomer, which is in turn polymerized to yield poly(methyl methacrylate). Heteropolyoxometalate acids and salts are also useful acid catalysts, and commercial processes based on both their strong acid and oxidation–reduction properties are used industrially [3,5,6].

The study of heteropolyoxometalates as oxidation–reduction catalysts usually involves compounds containing the Keggin-based anion $[PMo_{12}O_{40}]^{3-}$, or species derived from this anion by replacement of one or more of the framework (i.e. addendum) Mo(VI) ions by V(V) [3,5,6]. The (α-)$[PMo_{12}O_{40}]^{3-}$ ion has a central tetrahedrally coordinated phosphorus atom, surrounded by four groups of three edge-shared octahedra (i.e. Mo_3O_{13} subunits). These are linked in turn to each other through shared oxygen atoms and to the central PO_4 unit, giving a species with overall T_d symmetry [8]. Studies have also included the related Dawson structure, $[P_2Mo_{18}O_{62}]^{6-}$, which may be formed by fusion of two (formal) "$[PMo_9O_{31}]^{3-}$" subunits, each

* Corresponding author. Tel.: +61 2 49215479.
E-mail address: robert.burns@newcastle.edu.au (R.C. Burns).

1381-1169/$ – see front matter © 2004 Elsevier B.V. All rights reserved.
doi:10.1016/j.molcata.2004.05.017

of which may be obtained from a $[PMo_{12}O_{40}]^{3-}$ ion by loss of three MoO_3 groups, one each from three adjacent Mo_3O_{13} subunits [9]. The well-defined arrangement of the atoms in these anions, as well as the anion arrangements of the solid compounds (the secondary structure), makes them highly attractive for model studies of catalytic processes, as well as being commercial catalysts in their own right. Changes in the compounds can be made in one or more of the addendum atoms of the anion, as indicated above, as well as by variation of the central heteroatom and, more importantly, the counter cations. All of these changes affect their catalysis properties.

The majority of heterogeneous catalysis studies of the $[PMo_{12}O_{40}]^{3-}$ ion (and also $[PW_{12}O_{40}]^{3-}$) have involved the acid form and its salts containing monovalent cations [3,5,6]. However, some studies have been reported with divalent and trivalent cations [1,7,10–12]. The structures of these types of compounds, and the characterization of their surface and bulk properties, are not as well established as those of the acid and its monovalent salts. The latter, particularly the insoluble Cs^+, Rb^+, K^+ and NH_4^+ salts, have been extensively studied with regard to structure, pore size and pore distribution, etc. [7,13–16]. However, two fairly recent publications have suggested that soluble alkaline earth metal salts prepared by the reaction of $H_3[PMo_{12}O_{40}]$ (and also $H_3[PW_{12}O_{40}]$) and the alkaline earth hydroxides, which were characterized by infrared spectroscopy, X-ray powder diffraction (XRD), differential thermal analysis and nitrogen adsorption–desorption measurements, are, in fact, a mixture of simple divalent salts and the parent acid itself [17,18]. Moreover, a single-crystal X-ray structural investigation of the product obtained from the $Ba^{2+}/[PMo_{12}O_{40}]^{3-}$ system gave a unit cell effectively identical with that of the hydrated acid, $H_3[PMo_{12}O_{40}]\cdot(29–30)H_2O$ [18–20] and, furthermore, the Ba^{2+} ions could not be located within the unit cell, supporting the above conclusion.

Prior to any investigations of the heterogeneous catalysis behaviour of the putative alkaline earth metal salts of the $[PMo_{12}O_{40}]^{3-}$ ion, as well as to place previous catalysis studies employing these compounds on a firmer footing, the problem of the identities of these salts, as well as those of other aqueous soluble salts (i.e. those containing the Group 1 cations Li^+ and Na^+, and the Group 13 cations, such as Al^{3+}) needs to be resolved. Consequently, this paper reports on the preparation of solutions containing alkaline earth metal ions and the $[PMo_{12}O_{40}]^{3-}$ ion obtained by the reaction of the parent acid and alkaline earth metal carbonates (or hydroxide/carbonates), and other soluble $[PMo_{12}O_{40}]^{3-}$ salts, such as those containing the Li^+, Na^+ and Al^{3+} cations, together with the crystallization and chemical analysis of solids obtained from these solutions. Infrared spectroscopy, TGA/DTA studies, X-ray and neutron powder diffraction, and both solution and solid-state ^{31}P NMR spectroscopy are used to characterize the resulting solids.

2. Experimental

2.1. Preparation and characterization of solutions and crystallized solids containing the $[PMo_{12}O_{40}]^{3-}$ ion and the alkaline earth metal, alkali metal and Group 13 metal ions Mg^{2+}, Ca^{2+}, Sr^{2+}, Ba^{2+}, Li^+, Na^+ and Al^{3+}

In a typical preparation, 12.80 g (5.48 mmol) of $H_3[PMo_{12}O_{40}]\cdot\sim28H_2O$ (water content determined accurately by TGA) was dissolved in 12 mL of deionized water, followed by the slow addition over a period of about 10–15 min of finely-powdered, solid $(MgCO_3)_4\cdot Mg(OH)_2\cdot 5H_2O$ (exact composition determined by TGA; 0.746 g, 1.644 mmol) to give a 3:2 Mg^{2+}:$[PMo_{12}O_{40}]^{3-}$ mole ratio, with continuous stirring and gentle heating (30–40 °C). Each further addition of solid was made following complete reaction of the previous addition of carbonate/hydroxide to generate CO_2. For the preparations of the corresponding Ca^{2+}, Sr^{2+} and Ba^{2+} compositions the equivalent amounts of dried MCO_3 ($M = Ca^{2+}$, Sr^{2+}, Ba^{2+}) were used. On completion of the addition of the solid and following complete CO_2 generation, a further 3–5 mL of water was used to wash any splashed material from the sides of the beaker into the bulk, and the temperature of the resulting solution was raised to 50–60 °C for ∼5 min. This procedure always resulted in the formation of clear, bright yellow solutions. The solutions were then allowed to cool to room temperature. For the preparations of the Li^+ and Na^+ compositions the stoichiometry was adjusted to a 3:1 cation:$[PMo_{12}O_{40}]^{3-}$ mole ratio, using the same initial amount of acid, and the above procedure was followed using dried Li_2CO_3 and Na_2CO_3, respectively. In the case of Al^{3+}, 1.73 g (2.740 mmol) of solid $Al_2(SO_4)_3\cdot 16H_2O$ was added to the solution containing the acid to give a 1:1 cation:$[PMo_{12}O_{40}]^{3-}$ mole ratio, again with the same initial amount of acid. Solid $BaCO_3$ (1.62 g, 8.219 mmol) was then slowly added with continuous stirring and heating, as above, and the slurry was further heated to 50–60 °C after completion of CO_2 generation. On cooling the mixture was stirred for about 1–2 h and the solid $BaSO_4$ removed by filtration using a 0.45 μm filter. The solid was washed with a small amount of water (∼5 mL), which was combined with the original filtrate.

Solids from the above solutions were obtained by placing the solutions in 50 mL beakers, inside a vacuum dessicator containing dried silica gel and applying a vacuum (water pump vacuum for 10–15 min). Over a period of hours to days yellow crystals were obtained in each case, which were isolated while there was still solution covering the crystals. This can be as much as a 50% yield or greater, although the amount is not critical. These crystals were thoroughly dried between filter paper in each case and stored in closed vials at 0 °C, prior to chemical analysis, thermogravimetric and differential thermal analysis, infrared spectroscopy, solid-state and solution ^{31}P NMR spectroscopy

and X-ray powder diffraction. Infrared examination of the Al^{3+}-containing salt, $Al[PMo_{12}O_{40}]\cdot\sim30H_2O$, showed no evidence for the presence of SO_4^{2-} [a strong ν(SO) peak at $\sim1105\,cm^{-1}$].

The compound $(NH_4)_6[HPMo_{11}O_{39}]$ was prepared as originally described by Fournier and Massart [21], and exhibited peaks in the infrared spectrum (1200–400 cm^{-1}) at 1056, 1029 sh, 1003, 932, 897, 856, 793, 741, 593 and $\sim520\,cm^{-1}$. These values agree with those previously reported except for the additional shoulder observed in the present work at $1029\,cm^{-1}$ [22]. Note that the infrared spectroscopic data originally reported were attributed to the $[PMo_{11}O_{39}]^{7-}$ ion, not $[HPMo_{11}O_{39}]^{6-}$. The compound $(NH_4)_3[PMo_{12}O_{40}]$ was obtained commercially (Aldrich), while the preparation of $K_3[PMo_{12}O_{40}]$ has been reported previously [7].

Thermogravimetric and differential thermal analyses (TGA/DTA) were performed on a Stanton Redcroft TG-750 instrument coupled to a Eurotherm Model 94 temperature controller, or on a TA Instruments SDT 2960 Simultaneous DTA/TGA instrument. Sample masses of 10–50 mg were used, with a heating rate of 2 or 10 °C/min in a static air atmosphere or under a flow of air of 20 mL/min. In general the profiles of the TGA/DTA analyses run at the two heating rates were very similar. There was slightly better separation of the mass loss stages in the TGA at the lower heating rate, while in the DTA the endothermic peaks attributable to water loss were somewhat better resolved. Also, there was a small shift for both the exothermic and endothermic peaks in the DTA of between 10 and 15 °C to lower temperatures at the lower heating rate. All infrared (IR) spectra were recorded on a Bio-Rad FTS-7 Fourier-transform spectrophotometer ($2\,cm^{-1}$ resolution), with the samples mounted as KBr discs. X-ray powder diffraction was performed on a Philips PW1710 Automated Powder Diffractometer with a Philips PW1050 goniometer, using graphite-monochromated Cu Kα radiation. As the fully hydrated compounds readily lose water of crystallization on standing in the atmosphere, the materials were quickly ground using a mortar and pestle and placed in a holder with a surface covering of "cling wrap". The holder was then sealed so that no water could escape from the sample. The "cling wrap" had a strong broad peak centred at $2\theta = 11.4°$ ($d \approx 7.8$ Å) and a weaker, broad peak at $\sim20.0°$ ($d \approx 4.4$ Å), as well as a weak, sharp peak at 36.0° ($d \approx 2.5$ Å). Solution ^{31}P NMR spectra were obtained on a Bruker AVANCE DPX-300 spectrometer operating at 121.49 MHz, while solid-state ^{31}P NMR spectra were recorded on a Varian Inova 300 spectrometer operating at the same frequency, with high-powered proton decoupling. Samples were spun at 3.5 kHz and 16 scans were collected routinely for each sample. For solution studies 5 mm o.d. tubes were employed and the reference used was external 85% H_3PO_4, while for the solid-state studies $(NH_4)H_2PO_4$ was employed ($\delta = 1.00$, relative to 85% H_3PO_4).

2.2. Chemical analyses of crystallized solids of nominal composition $(M^{n+})_{3/n}[PMo_{12}O_{40}]$, where M^{n+} is a cation of a Group 1, 2 or 13 element

Chemical analyses of Li, Mg, Ca, Sr, Ba, Al and Mo in all solid samples were performed by inductively coupled plasma atomic emission spectroscopy (ICP-AES) or, in the case of Na, by flame photometry. Samples were dehydrated by heating at 300 °C for 4 h in an air atmosphere prior to analysis. Weighed amounts of each compound (~0.25 g) were dissolved in water (500 mL or 1 L, depending on the element) and slightly acidified using concentrated HNO_3. ICP-AES analyses were performed on an axial Varian Liberty Series II ICP-AES instrument controlled by Plasma 96 software. Multiple detection lines were used for each element, where possible. These included (values in nm) for Li (460.286, Li^0; 610.362, Li^0; 670.784, Li^0), Mg (279.553, Mg^+; 280.270, Mg^+; 285.213, Mg^0), Ca (393.366, Ca^+; 422.673, Ca^0), Sr (407.771, Sr^+), Ba (233.527, Ba^+; 389.178, Ba^+; 413.066, Ba^+), Al (394.401, Al^0) and Mo (281.615, Mo^+; 379.825, Mo^0; 386.411, Mo^0). Sodium was determined by flame photometry at 690 nm on a Corning 410 Flame Photometer. To avoid any potential chemical and/or physical interferences between the samples and standards, the standard addition method was employed in all ICP-AES and flame photometric analyses [23–25]. Concentrations for the standard addition analyses were chosen such that the absorbance/emission-concentration responses were always linear, and each determination involved four or five concentration points per graph (R^2 values for the plots were always >0.9995). Phosphorus analyses on samples, dried as described above, were performed by the Australian National University Microanalytical Laboratory, Canberra.

2.3. Neutron diffraction structure of $Ba_3[PMo_{12}O_{40}]_2\cdot\sim55D_2O$ by Rietveld powder analysis

A sample of $Ba_3[PMo_{12}O_{40}]_2\cdot\sim55D_2O$ was prepared using the crystallization method described above, except that the hydrated acid $\{H_3[PMo_{12}O_{40}]\cdot(28.6)H_2O$, 20.0 g, 8.54 mmol$\}$ was dried at 130 °C for 2 h in air prior to reaction and all work was performed in closed vessels using D_2O as the solvent. After dissolution of the anhydrous acid in about 30 mL of D_2O, dried $BaCO_3$ (2.53 g, 12.82 mmol) was added to the solution and the resulting mixture heated to about 70 °C. Following dissolution of the $BaCO_3$ a clear yellow solution resulted, which was allowed to crystallize overnight. The unfiltered sample was transported to the laboratories of ANSTO, Lucas Heights, Sydney, Australia and, following filtration, drying between filter paper and powdering using a mortar and pestle, was placed in a sealed vanadium can (12 mm o.d.). This was in turn placed inside a low-temperature cryostat controlled by an APD Cryogenics Inc. Heliplex, Model HC-4 Mk I, and the cryostat and sample mounted in the medium-resolution powder-diffraction beamline (MRPD) of the HIFAR nuclear reactor. The

sample was cooled to 150 K and the pattern recorded using a neutron wavelength of 1.6653(1) Å from about 5–140°, with a step size of 0.1°. The structure was refined using the program RIETICA [26], beginning with the anion atom coordinates previously reported for the X-ray structure of a crystal obtained from the $Ba^{2+}/[PMo_{12}O_{40}]^{3-}$ system [18]. All anion positional parameters were refined, and isotropic temperature factors were used for all atoms. Several O atoms in the water molecules were located and refined, most with partial occupancy. The background was refined using a 12-term Chebyshev polynomial function, and linewidths using a Voigt model.

Subsequent TGA studies on a sample of the crystallized material gave the composition $Ba_3[PMo_{12}O_{40}]_2{\cdot}(55.3)D_2O$ up to 400 °C. Chemical analysis, after drying at 300 °C for 4 h, gave %Ba, %P and %Mo compositions of 9.66, 1.60 and 55.6%, respectively (theoretical values: 10.16, 1.53 and 56.8%, respectively).

2.4. Density functional calculations

Density functional calculations on the $[PMo_{12}O_{40}]^{3-}$ ion to obtain the electrostatic and Mulliken charges of the oxygen atoms were performed using Spartan, Version 5.1 (Wavefunction Inc., Irvine, CA, USA), on a Silicon Graphics O2 workstation. The calculations were made for the ground state of the anion using a BP86 functional with self-consistent non-local corrections and a numerical DN basis set. The atomic coordinates of the $[PMo_{12}O_{40}]^{3-}$ ion were taken from the actual crystallographically-determined geometry (which has T_d symmetry) that is found in the structure of $H_3[PMo_{12}O_{40}]{\cdot}{\sim}29H_2O$ [19,20].

3. Results and discussion

3.1. Preparation of solutions and characterization of crystallized solids of nominal composition $(M^{n+})_{3/n}[PMo_{12}O_{40}]{\cdot}xH_2O$, where M^{n+} is a cation of a Group 1, 2 or 13 element

3.1.1. Synthesis

A series of aqueous solutions of compounds of nominal formula $M_3[PMo_{12}O_{40}]_2$ ($M = Mg^{2+}$, Ca^{2+}, Sr^{2+}, Ba^{2+}), $M'_3[PMo_{12}O_{40}]$ ($M' = Li^+$, Na^+), and $Al[PMo_{12}O_{40}]$ were prepared by reaction of $(MgCO_3)_4{\cdot}Mg(OH)_2{\cdot}5H_2O$ or the respective carbonates (MCO_3, $M = Ca^{2+}$, Sr^{2+} and Ba^{2+}; M'_2CO_3, $M' = Li^+$ and Na^+) with $H_3[PMo_{12}O_{40}]{\cdot}{\sim}28H_2O$ (water content determined by TGA) or, for the last compound, by combination of $Al_2(SO_4)_3{\cdot}16H_2O$ and $H_3[PMo_{12}O_{40}]{\cdot}{\sim}28H_2O$ in the appropriate stoichiometry, followed by addition of the requisite amount of $BaCO_3$ and subsequent removal by filtration of insoluble $BaSO_4$. The resulting solutions were clear, bright yellow in colour, and typically had pH values of 1.2–1.5 under the conditions of their preparation. As the H^+ of the original acid has been formally neutralized in these preparations, the acidic nature of the solutions indicates that the $[PMo_{12}O_{40}]^{3-}$ ion had hydrolysed, a well known phenomenon [8,27]. This was evident from the ^{31}P NMR of the solutions. A typical example is that of the $Mg^{2+}/[PMo_{12}O_{40}]^{3-}$ system, which showed the major anion, $[PMo_{12}O_{40}]^{3-}$, as well as several hydrolysis products including α-$[PMo_{11}O_{39}]^{7-}$ (likely as its mono- and di-protonated forms), α-$[P_2Mo_{18}O_{62}]^{6-}$, and α-A-$[PMo_9O_{31}(OH)(H_2O)_2]^{4-}$ (likely as its protonated form). The distribution of species in this system is given in Table 1, based on the chemical shifts of the species previously identified in the $H^+/MoO_4^{2-}/HPO_4^{2-}$ system [28], and the actual integrated intensities of the ^{31}P signals of the species observed in the $Mg^{2+}/[PMo_{12}O_{40}]^{3-}$ system. Over 80% of the phosphorus-containing species exist in the form of the $[PMo_{12}O_{40}]^{3-}$ ion. Interestingly, there was little α-$[P_2Mo_{18}O_{62}]^{6-}$ despite the presence of a large percentage of its monomeric precursor, α-A-$[PMo_9O_{31}(H_2O)_3]^{3-}$. The relatively slow formation of α-$[P_2Mo_{18}O_{62}]^{6-}$ as a result of dimerization of two monomeric precursor units has been noted previously [28]. The chemical shifts of the species observed in the $Mg^{2+}/[PMo_{12}O_{40}]^{3-}$ system were all slightly different to those reported in the $H^+/MoO_4^{2-}/HPO_4^{2-}$ system, generally appearing 0.4–0.5 ppm to higher frequencies (i.e. a more positive chemical shift). This may be attributed to possible ion pairing, resulting in deshielding of the phosphorus environment in the observed anions. Similar, more positive chemical shifts were also observed for all of the other Group 1, 2 and 13/$[PMo_{12}O_{40}]^{3-}$ systems. A comprehensive discussion of chemical shift variations for polyoxometalate ions in solution, particularly in relation to the diamagnetic susceptibility of the solvent, has been previously presented [29]. All solution spectra in this study were obtained under similar conditions.

When the solutions were allowed to evaporate slowly under vacuum in a dessicator over silica gel, yellow crystals formed in each case over a period of hours to days. The rate of formation of the crystals depended on the cation, and followed the order given below (fastest crystallization first):

$$Ba^{2+} > Sr^{2+} > Ca^{2+} > Mg^{2+} > H^+.$$

The H^+ has been included for comparative purposes. The two alkali metals formed crystals much more slowly than did Mg^{2+}, with Na^+ faster than Li^+, and both faster than H^+. Al^{3+} generated crystals more quickly than did Mg^{2+}, but slower than Na^+. The relative rates of crystallization are reproducible. All crystals were isolated, quickly dried between filter paper and subsequently stored at 0 °C. The resulting crystals were highly hydrated and readily lost water on standing at room temperature in the air, generating lower hydrates. Given the ease of loss of the water of crystallization, it is likely that much of the water is zeolitic-like in nature.

Table 1
^{31}P NMR data on the $Mg^{2+}/[PMo_{12}O_{40}]^{3-}$ system prepared by addition of solid $(MgCO_3)_4{\cdot}Mg(OH)_2{\cdot}5H_2O$ to aqueous $H_3[PMo_{12}O_{40}]$

Species[a]	Chemical shift, δ (ppm)	Integrated intensity	Species % based on ^{31}P distribution
α-$[PMo_{12}O_{40}]^{3-}$ (I)	−2.73	1.00	80.3
α-$[P_2Mo_{18}O_{62}]^{6-}$ (H)	−2.03	0.012	0.5
F (with Mo/P > 12)	−1.33	0.015	1.2
$[PMo_{11}O_{39}]^{7-}$ and protonated forms (D)	−0.71	0.201 (combined species D and E)	16.1 (combined species D and E)
α-A-$[PMo_9O_{31}(OH)(H_2O)_2]^{4-}$ and protonated form (E)	−0.60		
Protonated forms of α-B-$[PMo_9O_{34}]^{9-}$ (B)[b]	0.55	0.024	1.9

[a] Alphabetical symbol designation according to reference [28].
[b] Suggested structure [28].

3.1.2. TGA/DTA and elemental analysis

The above solids were analysed for their elemental composition and water content, the latter by TGA. Assuming that the solids that were isolated contain the stoichiometric compounds indicated above, the water of crystallization for the alkaline earth metal salts, the alkali metal salts and the Al^{3+} salt all exhibited about 27–31 H_2O molecules per $[PMo_{12}O_{40}]^{3-}$ ion, and are similar to that found for the free acid. The data are given in Table 2. The TGA results for the Na^+-, Mg^{2+}- and Al^{3+}-containing solids are shown in Fig. 1, along with that for the hydrated acid $H_3[PMo_{12}O_{40}]{\cdot}{\sim}28H_2O$. While lower hydrates of the acid are known, such as $H_3[PMo_{12}O_{40}]{\cdot}(13–14)H_2O$ [30], the fully hydrated parent acid has been reported to have 29–30 H_2O molecules per $[PMo_{12}O_{40}]^{3-}$ ion, although only a limited number of these were crystallographically located in a single-crystal X-ray study [19,20]. Routinely, it was observed that there were only 28–29 H_2O molecules per $[PMo_{12}O_{40}]^{3-}$ ion as determined by TGA for commercially obtained samples of the free acid. Likewise, the alkaline earth metal salts have been reported to have 58 water molecules of crystallization per formula unit, i.e. $M_3[PMo_{12}O_{40}]_2{\cdot}58H_2O$, or 29 per $[PMo_{12}O_{40}]^{3-}$ ion [31,32]. From the present data, there was little difference between the mass losses for the various salts, and no apparent trend among the three different groups (i.e. Groups 1, 2 and 13). The variations in water content were likely caused by the extent to which the samples were dried when originally prepared.

The variations in the rates of crystallization of the solids from solution suggest the influence of the cations that are present in solution. Consequently, chemical analyses were performed on the crystallized solids for both cation and molybdenum content by ICP-AES, after drying at 300 °C for 4 h, while sodium was analysed by flame photometry. All metal analyses were performed using the standard addition method, to eliminate potential interference problems [23–25]. Phosphorus analyses were obtained commercially, again after drying as described above. The data are listed in Table 3. All metal (i.e. cation and Mo) and phosphorus atom percentage results show that the formulae of the solids are close to those expected for the dehydrated salts of composition $(M^{n+})_{3/n}[PMo_{12}O_{40}]$, where M^{n+} is a cation of a Group 1, 2 or 13 element. In the ICP-AES analyses there were some slight variations between determinations using multiple detection lines for an element, but these differed by no more than 3.3%, the maximum observed in the case of lithium. The majority of determinations generally gave significantly better agreement. These variations were greater than the standard errors in the actual % composition values.

While the TGA results have been discussed above, further insight into the composition of the crystallized solids

Table 2
Thermogravimetric (TGA) and differential thermal analysis (DTA) data for the hydrated acid and nominal salts of the $[PMo_{12}O_{40}]^{3-}$ ion

Compound (hydrated)	H_2O/anion (TGA)	H_2O/anion (lit.)[a,b,c]	DTA endotherms (°C)[d,e]	DTA exotherms (°C)[d,e]
$H_3[PMo_{12}O_{40}]$	∼28–29[f]	29–30	–	–
$Mg_3[PMo_{12}O_{40}]_2$	30.2	29	130 m, 150 w, 325 w, 355 w, 375 w	430 w, br
$Ca_3[PMo_{12}O_{40}]_2$	30.8	29	200 w, 325 s, 365 w	420 w, 445 m, 565 w, br
$Sr_3[PMo_{12}O_{40}]_2$	29.5	29	140 s, 165 w, 270 m, br	425 m, 530 w
$Ba_3[PMo_{12}O_{40}]_2$	27.4	29	185 w, br, 263, m	450 w, br
$Li_3[PMo_{12}O_{40}]$	27.4	–	–	–
$Na_3[PMo_{12}O_{40}]$	28.6	–	–	–
$Al[PMo_{12}O_{40}]$	30.0	–	–	–

[a] From [19].
[b] From [31].
[c] From [32].
[d] From [17].
[e] From [18].
[f] Commercial samples.

Table 3
Analytical data on the nominal $(M^{n+})_{3/n}[PMo_{12}O_{40}]$ salts of selected Group 1, 2 and 13 elements

Compound[a]	Cation			Phosphorus		Molybdenum		
	Line (nm)	Observed (%)[b]	Calculated (%)[b]	Observed (%)[b]	Calculated (%)[b]	Line (nm)	Observed (%)[b]	Calculated (%)[b]
$Li_3[PMo_{12}O_{40}]$	460.3	1.16	1.13	1.70	1.68	281.6	61.3	62.5
	670.8	1.24	1.13			379.8	60.5	62.5
$Na_3[PMo_{12}O_{40}]$	690	3.3	3.65	1.79	1.64	379.8	62.0	60.9
						386.4	60.6	60.9
$Mg_3[PMo_{12}O_{40}]_2$	279.6	1.72	1.96	1.74	1.67	281.6	63.7	61.9
	280.3	1.72	1.96			379.8	61.8	61.9
	285.2	1.76	1.96					
$Ca_3[PMo_{12}O_{40}]_2$	393.4	3.45	3.19	1.72	1.65	379.8	61.9	61.2
	422.7	3.37	3.19			386.4	62.5	61.2
$Sr_3[PMo_{12}O_{40}]_2$	407.8	6.42	6.73	1.46	1.59	379.8	56.6	58.9
						386.4	56.7	58.9
$Ba_3[PMo_{12}O_{40}]_2$	233.5	9.66	10.16	1.55	1.53	281.6	55.8	56.8
	389.2	9.38	10.16			379.8	53.6	56.8
	413.1	9.22	10.16					
$Al[PMo_{12}O_{40}]$	394.4	1.61	1.46	1.72	1.67	379.8	61.5	62.3
						386.4	64.0	62.3

[a] Water content not included in the formulation.
[b] Percentage based on dried compound (heated at 300 °C for 4 h).

comes from a consideration of the profiles of the TGA traces in conjunction with the DTA studies, as shown in Fig. 1. Some data on these compounds are also given in Table 2. For the free acid $H_3[PMo_{12}O_{40}]\cdot\sim28H_2O$ (Fig. 1(a)), the water of crystallization was lost in several strongly endothermic steps up to 160–170 °C to yield anhydrous $H_3[PMo_{12}O_{40}]$. This was followed by a further ∼1.5% loss in mass from ∼370–440 °C, with a weak, broad endothermic peak centred at ∼421 °C, which was terminated by an exothermic peak located at ∼438 °C. The ∼1.5% mass loss has been attributed to the successive formation of the anhydride phase $H_x[PMo_{12}O_{38.5+x/2}]$ ($x = \sim0.1$) and then an oxide phase $(PMo_{12}O_{38.5})_n$, both following loss of "constitutional" water [33,34]. At higher temperatures an exothermic peak was located at 509 °C, which must involve a phase change as there is no associated loss in mass, while the products MoO_3 (with an ∼0.01 P content) and $(MoO_2)_2P_2O_7$ have been reported to form at higher temperatures [33].

Comparison of the TGA and DTA profiles for the Na^+-, Mg^{2+}- and Al^{3+}-containing solids (Fig. 1(b)–(d), respectively) shows that they are quite different from that of $H_3[PMo_{12}O_{40}]\cdot\sim28H_2O$. This is especially evident in the case of the Na^+- and Al^{3+}-containing salts. For the Na^+ salt, the water of crystallization was lost in a large endothermic step from room temperature up to ∼120 °C, with a further endothermic step at 223 °C. No further mass loss was observed up to ∼600 °C, although exothermic and endothermic peaks were observed at 421 and 510 °C. The former corresponds to thermal decomposition of the compound, while the latter is likely associated with a phase change of a decomposition product, perhaps Na_3PO_4. The thermal decomposition of the compound was established in a separate study by X-ray powder diffraction examination of the solid following heating in an air atmosphere at 450 °C.

For the Al^{3+} salt, the water of crystallization was lost in two major endothermic stages, from room temperature to ∼140 °C, and from 140 to ∼300 °C. There appear to be two minor endothermic peaks at ∼240 and ∼286 °C, associated with water loss, followed by a major exothermic peak at 388 °C. The latter does not have any associated mass loss and must be a phase change, corresponding to thermal dissociation of the solid. Again, this was established by XRD examination of the solid following heating at 420 °C in air. No further mass losses occurred up to ∼600 °C. Most importantly, for the Na^+- and Al^{3+}-containing salts there was no evidence for mass losses or associated peaks in the DTA profiles from ∼370 to 440 °C. These would certainly be observable if the solids that crystallized from solution each consisted of a two-phase system containing both the free acid and a (poorly crystalline or amorphous) Na^+- or Al^{3+}-containing salt (perhaps another phosphopolyoxomolybdate or polyoxomolybdate), by analogy with the suggestion made by McGarvey et al. [17,18]. Strictly speaking, this suggestion was made only for the alkaline earth metal cation systems, but should be applicable to any crystallized solid obtained with the Group 1, 2 and 13 cations, all of which have soluble $[PMo_{12}O_{40}]^{3-}$ salts that are prepared using essentially the same synthetic approach.

For the Mg^{2+}-containing salt the TGA profile was less informative, as the water of crystallization was not completely lost until ∼420 °C. The maximum temperature at which water loss was complete for this solid was significantly

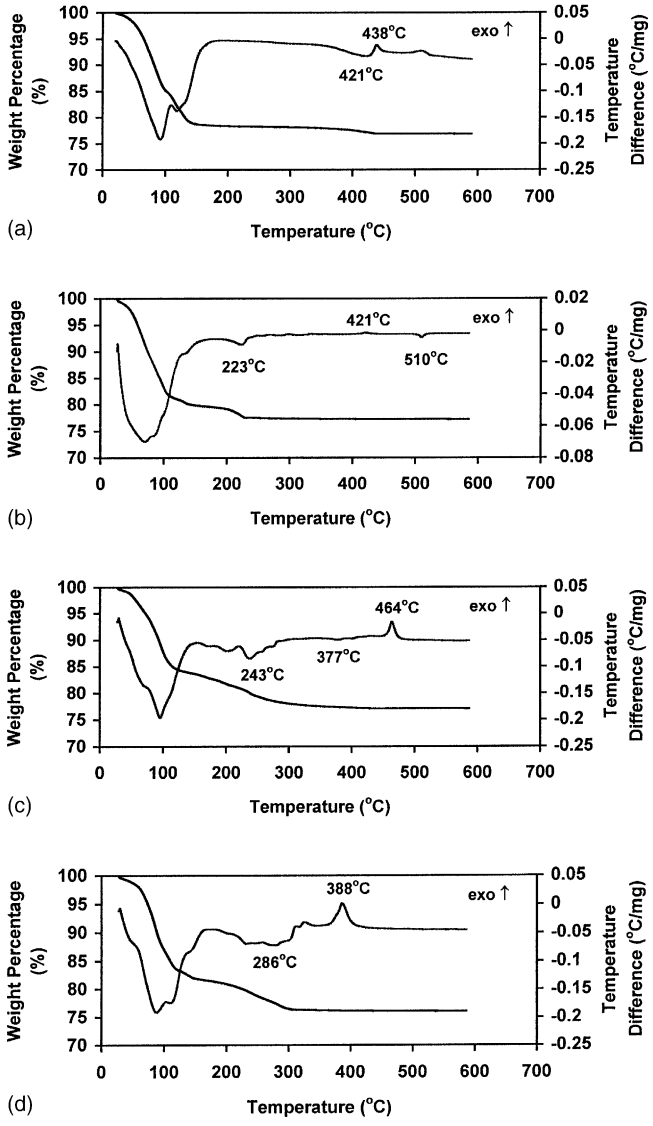

Fig. 1. Thermogravimetric analysis–differential thermal analysis traces of (a) $H_3[PMo_{12}O_{40}]\cdot\sim 28H_2O$, (b) $Na_3[PMo_{12}O_{40}]\cdot\sim 29H_2O$, (c) $Mg_3[PMo_{12}O_{40}]_2\cdot\sim 58H_2O$ and (d) $Al[PMo_{12}O_{40}]\cdot\sim 29H_2O$ from room temperature to 600 °C (heating rate 10 °C/min, air atmosphere, flow rate = 20 mL/min).

higher than that of the free acid and both the Na^+- and Al^{3+}-containing salts. It should be noted that it is also greater than that for the loss of "constitutional" water from the acid. Under identical experimental conditions, the order of retention of the water of crystallization for the three solids follows the trend $Mg^{2+} > Al^{3+} > Na^+$. This trend is not in agreement with that expected based on simple Coulombic attraction between the cations and water molecules, or on the rate of exchange of water molecules around the cations as found in aqueous solution. For Al^{3+}, Mg^{2+} and Na^+, the rate constants are 10^0, 10^5 and $>10^8\ s^{-1}$, respectively [35], which might be expected to reflect the tenacity of the cations to hold onto any coordinated water molecules. The above order is therefore likely related to the solid-state structures and stabilities of any lower hydrates that may be formed in these systems. These lower hydrates are suggested by the plateaus observed in the TGA profiles of the three salts. The DTA profile of the Mg^{2+}-containing salt was also different, showing endotherms at 98, 177, 207, 243, 263 and 278 °C, and a weak broad endotherm at ∼377 °C. All of these are associated with a loss of mass and hence loss of water of crystallization. These endotherms are followed by a strong exothermic peak at 464 °C, which corresponds to thermal decomposition of the solid, as established by XRD examination of the solid obtained following heating at 480 °C in air. The decomposition temperature obtained from the TGA/DTA study in the present work is in agreement with that obtained by Eguchi et al. [36] from the appearance of an exothermic peak at 427 °C, and the value of 430 °C of McGarvey et al. [17,18] obtained similarly. However, the endotherms observed in the present study are somewhat different to those found in the latter study, which are given in Table 2. Notably, not one of the distinctive peaks in the DTA profiles of the Na^+-, Mg^{2+}- and Al^{3+}-containing solids obtained in this study corresponds to any of those observed for the free acid, as would be expected to occur if the scenario of McGarvey et al. [17,18] was correct. This suggests that the acid did not crystallize to any significant extent during the isolation of these compounds.

3.1.3. *Infrared studies and density functional calculations*

Infrared spectroscopic data on the crystallized solids are given in Table 4, along with data on both the hydrated parent acid and on $[(n\text{-}C_4H_9)_4N]_3[PMo_{12}O_{40}]$. In addition to the broad ν(O–H) and δ(H–O–H) peaks at ∼3420 and ∼1635 cm^{-1} from the water of crystallization, all spectra of the crystallized solids exhibited four peaks that are characteristic of the $[PMo_{12}O_{40}]^{3-}$ ion [37,38] but are, in fact, complex in their makeup.

The vibrational representation of an isolated $[XM_{12}O_{40}]^{n-}$ ion of T_d symmetry with the Keggin structure is given by [37]:

$$\Gamma_{vib} = 9A_1 + 4A_2 + 13E + 16T_1 + 22T_2$$

Of these, only the $22T_2$ modes are infrared active and are triply degenerate. The four observed infrared-active bands for the $[PMo_{12}O_{40}]^{3-}$ ion have been assigned previously as ν_{as}(P–O_a), ν_{as}(Mo–O_b–Mo), ν_{as}(Mo–O_c–Mo) and ν_{as}(Mo=O_d), where O_a is an internal oxygen atom of the central XO_4 group, O_b and O_c are bridging oxygen atoms that are located between, i.e. linking, and within the Mo_3O_{13} subunits, and O_d is a terminal oxygen atom [37,38].

The spectra of all solids were almost identical in both the P–O and Mo–O stretching regions, and there was no evidence for the presence of either the $[P_2Mo_{18}O_{62}]^{6-}$ or lacunary $[HPMo_{11}O_{39}]^{6-}$ ions in the spectra. The presence of $[P_2Mo_{18}O_{62}]^{6-}$ would be apparent from the appearance of two ν_{as}(P–O) stretches at ∼1077 (s) and ∼1002 (m) cm^{-1} {the local symmetry around each PO_4 group in $[P_2Mo_{18}O_{62}]^{6-}$ is C_{3v} rather than T_d as in $[PMo_{12}O_{40}]^{3-}$,

Table 4
Infrared data (cm^{-1}) on hydrated (~$29H_2O$/anion) and dried (at 125 °C under vacuum) salts of the type $(M^{n+})_{3/n}[PMo_{12}O_{40}]$ containing selected Group 1, 2 and 13 cations, and H^+ and $[(n\text{-}C_4H_9)_4N]^+$

Compound	ν_{as}(P–O_a)	ν_{as}(Mo=O_d)[a]	ν_{as}(M–O_b–M)	ν_{as}(M–O_c–M)[a]
$[(n\text{-}C_4H_9)_4N]_3[PMo_{12}O_{40}]$	1061	962 sh, 953	879	806 br
$H_3[PMo_{12}O_{40}]\cdot\sim28H_2O$	1063	972 sh, 961	870	785 br
$H_3[PMo_{12}O_{40}]$ dried	1063	972 sh, 960	867	784 br
$Li_3[PMo_{12}O_{40}]\cdot\sim29H_2O$	1063	973 sh, 961	870	785 br
$Li_3[PMo_{12}O_{40}]$ dried	1063	972 sh, 960	867	785 br
$Na_3[PMo_{12}O_{40}]\cdot\sim29H_2O$	1062	972 sh, 961	868	784 br
$Na_3[PMo_{12}O_{40}]$ dried	1064	972 sh, 960	866	785 br
$Mg_3[PMo_{12}O_{40}]_2\cdot\sim58H_2O$	1063	973 sh, 960	870	782 br
$Mg_3[PMo_{12}O_{40}]_2$ dried	1063	972 sh, 960	866	783 br
$Ca_3[PMo_{12}O_{40}]_2\cdot\sim58H_2O$	1063	973 sh, 961	870	785 br
$Ca_3[PMo_{12}O_{40}]_2$ dried	1064	973 sh, 960	867	783 br
$Sr_3[PMo_{12}O_{40}]_2\cdot\sim58H_2O$	1063	973 sh, 960	870	786 br
$Sr_3[PMo_{12}O_{40}]_2$ dried	1064	973 sh, 960	867	784 br
$Ba_3[PMo_{12}O_{40}]_2\cdot\sim58H_2O$	1063	973 sh, 961	870	787 br
$Ba_3[PMo_{12}O_{40}]_2$ dried	1064	973 sh, 960	868	785 br
$Al[PMo_{12}O_{40}]\cdot\sim29H_2O$	1063	972 sh, 961	869	785 br
$Al[PMo_{12}O_{40}]$ dried	1064	972 sh, 960	867	784 br

[a] sh: shoulder, br: broad.

causing splitting of the triply degenerate ν_{as}(P–O) stretch ν_3, $T_2 \rightarrow A_1 + E\}$, as well as an ν_{as}(Mo=O) stretch at ~965 (s) cm^{-1} and several ν_{as}(Mo–O–Mo) stretches at ~940 (s), ~905 (vs), ~835 (s) and ~785 (vs) cm^{-1} [9,39]. In general, these peaks do not overlap with those of the $[PMo_{12}O_{40}]^{3-}$ ion, and are easily observed.

Similarly, the $[HPMo_{11}O_{39}]^{6-}$ ion in $(NH_4)_6[HPMo_{11}O_{39}]$ exhibits ν_{as}(P–O) stretches at 1056 (s) (with a shoulder at 1029) and 1003 (m) cm^{-1}, two ν_{as}(Mo=O) stretches at 932 (s) and 897 (s) cm^{-1} and broad ν_{as}(Mo–O–Mo) stretches at 856 (s), 793 (s) and 741 (s) cm^{-1}. While there is some overlap with the bands of the $[PMo_{12}O_{40}]^{3-}$ ion, the presence of this anion also would be easily apparent. The absence of the bands characteristic of the $[P_2Mo_{18}O_{62}]^{6-}$ and lacunary $[HPMo_{11}O_{39}]^{6-}$ ions indicates that the crystallized compounds contained none or very little of these species, which are the most likely phosphorus-containing polyoxomolybdate impurity anions.

The variations in the positions of the four characteristic IR bands have been discussed previously [37,38], and arise from the effects of various interactions between the anions themselves, and with the attendant cations and any water molecules of crystallization that are present. Interestingly, the ν_{as}(Mo=O_d) band always has a shoulder to higher frequencies, while the ν_{as}(Mo–O_c–Mo) band is always very broad. In either case this may presumably be attributed to splitting of the triply degenerate components that make up these bands, likely by interactions with the cations and water molecules.

Previously, the trends in the positions of these four bands were established by comparison with cation systems that were very poorly polarizing (and hence not involved in hydrogen bonding), and which forced the anions apart, thereby eliminating any interactions between them [38]. For this purpose the tetraalkylammonium cations were used, and it was shown that with four or more carbon atoms in the alkyl chain no further shifts in the IR active modes occurred, indicating that the anions were effectively isolated. Data for the $(n\text{-}C_4H_9)_4N^+$ salt are therefore included in Table 4.

In general, the ν_{as}(Mo=O_d) mode, which is effectively a purely stretching vibration, always increases with increasing closeness of the anions as a result of (repulsive) Coulombic interactions (i.e. an increased electrostatic potential field arising from the presence of the negatively charged oxygen atoms of surrounding anions making it more difficult for this peripheral stretch to occur). However, the original analysis did not consider the effects of interactions with polarizing cations or water molecules, both of which would lead to a decrease in frequency. This arises from electron donation from the lone pairs of the terminal oxygen atoms of the anion to either a polarizing cation or interaction with a hydrogen atom of a water molecule to generate a hydrogen bond. In each case this will result in a weakening of the Mo=O bond and a decrease in stretching frequency. The fact that decreases are never observed for the ν_{as}(Mo=O_d) mode indicates that Coulombic effects are always preeminent for this vibration.

The ν_{as}(Mo–O_b–Mo) and ν_{as}(Mo–O_c–Mo) bands are not pure stretching vibrations, but contain some bending character in addition to their primary stretching contribution [38]. The effects of decreasing interanionic distances, together with interactions with cations and water molecules can lead to opposite influences on these bands [38]. Increases in electrostatic anion–anion interactions will lead to increases in

the stretching frequency contribution of these bridging vibrations, as described above, but have an opposite effect on the bending contribution of these bands. Moreover, any cation–anion interactions and water–anion interactions will also lead to a decrease in frequency for these vibrations. For the ν_{as}(Mo–O_c–Mo) band decreasing frequencies are always observed compared to the $(n\text{-}C_4H_9)_4N^+$ salt (i.e. a cation system with isolated anions), while the ν_{as}(Mo–O_b–Mo) band shows greater variation, and may either increase or decrease in frequency depending on the nature of the cation system [38]. The ν_{as}(P–O_a) stretch does not depend greatly on the counter cation, although this is not true for other central heteroatoms, such as As(V), Si(IV) and Ge(IV) [38].

Examination of the data in Table 4 indicates that, relative to $[(n\text{-}C_4H_9)_4N]_3[PMo_{12}O_{40}]$, both the hydrated acid and the hydrated salts always show an increase in frequency for the ν_{as}(Mo=O_d) mode, of about 7–8 cm^{-1}, while ν_{as}(P–O_a) shows little variation ($\pm 2\,cm^{-1}$), as expected. Both ν_{as}(Mo–O_b–Mo) and ν_{as}(Mo–O_c–Mo) decrease in frequency, showing shifts of about 9–11 and 21–24 cm^{-1}, respectively, indicating that there are significant interactions of both O_b and O_c with the cations and with the hydrogen atoms of the water molecules of crystallization. It is a little surprising that the decreases in frequency relative to $[(n\text{-}C_4H_9)_4N]_3[PMo_{12}O_{40}]$ are so great for these bands given the ease of removal of much of the water, as noted above. However, the individual influences on these bands are complex, as previously discussed. When the samples (already mounted as KBr discs) were gently dehydrated by heating at 125 °C under vacuum for about 4 h, some further minor shifts were noted. While neither ν_{as}(Mo=O_d) nor ν_{as}(P–O_a) varied to any great extent, there was a further decrease for the ν_{as}(Mo–O_b–Mo) mode of about 2–4 cm^{-1}, while ν_{as}(Mo–O_c–Mo) showed little variation, with only small increases or decreases in wavenumber compared to their respective fully hydrated compounds. Dehydration would result in the elimination of the hydrogen-bonding network between the water molecules and oxygen atoms of the $[PMo_{12}O_{40}]^{3-}$ ions, likely increasing the Coulombic potential by collapsing the three-dimension structure of the solid. However, this increase in Coulombic potential is not supported by the lack of change in the ν_{as}(Mo=O_d) frequency. Thus the decrease in the ν_{as}(Mo–O_b–Mo) frequency suggests preferential strong interactions of the O_b atoms of the anion with a polarizing counter cation(s) relative to the O_c and O_d atoms, based on the frequency shifts observed on dehydration. It is also possible that any potential increase in the ν_{as}(Mo=O_d) frequency is negated by a corresponding decrease through greater interaction of the O_d atoms with the cations.

Density functional calculations on an isolated $[PMo_{12}O_{40}]^{3-}$ ion indicate that the relative electrostatic and Mulliken charges (the latter in parentheses) on the O_b, O_c and O_d atoms are −0.53 (−0.68), −0.54 (−0.60) and −0.47 (−0.37), respectively, with the internal O_a atoms −0.77 (−0.94). For O_b and O_c there is a reversal between the calculated electrostatic and Mulliken charges and, while the former should provide a better indication of the attraction of an external positive charge (i.e. a cation) for an oxygen atom, the electrostatic charges for O_b and O_c are almost the same. The calculated electrostatic and Mulliken charges for both O_b and O_c are more negative than that of the terminal O_d atoms, while the most negative oxygen atoms are the internal, but inaccessable, O_a atoms. Based on these calculations it would therefore be most likely that the cations would associate with the bridging O_b and O_c oxygen atoms, as is observed. This could be subject to stereochemical considerations that depend on the relative numbers of cations per $[PMo_{12}O_{40}]^{3-}$ anion, which is related to the actual cation charge, and also their distribution in the dehydrated structure. This may account for the slight observed preference for the bridging O_b oxygen atoms on dehydration. Thus, while there is IR evidence for the effects of the presence of cations in the structure, no actual trends in the frequencies of the $[PMo_{12}O_{40}]^{3-}$ ion with variation in the cations from Groups 1, 2 and 13 could be discerned.

3.1.4. ^{31}P *solution and solid-state NMR studies*

It is possible that co-crystallization of, for example, the lacunary hydrolysis products $[HPMo_{11}O_{39}]^{6-}$ and $[PMo_9O_{31}(OH_2)_3]^{3-}$, possibly in one or more differently protonated forms, could occur during the fractional crystallization process. Indeed, in related heteropolyoxotungstate chemistry, it is well known that salts of the lacunary species $[PW_{11}O_{39}]^{7-}$, and also transition metal-substituted salts of this anion, often crystallize with an almost identical unit cell and structure as the $[PW_{12}O_{40}]^{3-}$ salts, with the anion exhibiting positional disorder such that the vacant "WO^{4+}" (or transition metal-substituted) site cannot be crystallographically located. In order to explore the possibility of co-crystallization of the (protonated) $[PMo_{11}O_{39}]^{7-}$ ion and/or other hydrolysis products during crystallization, solid-state ^{31}P NMR studies were carried out on $H_3[PMo_{12}O_{40}]\cdot\sim 28H_2O$ and the fully hydrated salts with Na^+, Mg^{2+} and Al^{3+} counter cations. Following crystallization of the solid in each case, the filtered crystals were washed with a small amount of ice-cold water to remove any liquid adhering to the crystals, which would contain soluble (i.e. non-co-crystallized) hydrolysis products, if present. The solids were then dried with filter paper, and stored at <0 °C to avoid water loss. The data are given in Table 5, and the solid-state ^{31}P NMR spectra of $H_3[PMo_{12}O_{40}]\cdot\sim 28H_2O$ and $Mg_3[PMo_{12}O_{40}]_2\cdot\sim 58H_2O$ shown in Fig. 2.

For all four solids, the major signal came from the $[PMo_{12}O_{40}]^{3-}$ ion, and occurred from about −3.5 to −5 ppm [$(NH_4)H_2PO_4$, $\delta = 1.00$ ppm]. A trend to more positive chemical shifts relative to $H_3[PMo_{12}O_{40}]\cdot\sim 28H_2O$ can be observed with increasing charge on the cation for Na^+ and Mg^{2+}, but decreases again for Al^{3+}. This variation implies that Group 1, 2 or 13 cations must be present in the structures of these compounds and associated with the $[PMo_{12}O_{40}]^{3-}$ ions, and also indicates the effects that

Table 5
Solid-state and solution (in d_6-DMSO) ^{31}P NMR data on $H_3[PMo_{12}O_{40}]\cdot\sim28H_2O$ and compounds of the type $(M^{n+})_{3/n}[PMo_{12}O_{40}]\cdot\sim29H_2O$, where $M^{n+} = Na^+$, Mg^{2+} and Al^{3+}

Compound	Anion	Solid-state δ (ppm) [$(NH_4)H_2PO_4$ = 1.00 ppm]	Solution (d_6-DMSO)	
			δ (ppm)	Integral
$H_3[PMo_{12}O_{40}]\cdot\sim28H_2O$	$[PMo_{12}O_{40}]^{3-}$	−4.75	–	–
$Na_3[PMo_{12}O_{40}]\cdot\sim29H_2O$	$[PMo_{12}O_{40}]^{3-}$	−4.09	−2.99	1.00
	$[H_2PMo_{11}O_{39}]^{5-}$	–	−0.23	0.16
$Mg_3[PMo_{12}O_{40}]_2\cdot\sim58H_2O$	$[PMo_{12}O_{40}]^{3-}$	−3.70	−3.38	1.00
	$[H_2PMo_{11}O_{39}]^{5-}$	–	−0.66	0.19
$Al[PMo_{12}O_{40}]\cdot\sim29H_2O$	$[PMo_{12}O_{40}]^{3-}$	−4.12	−2.97	1.00
	$[H_2PMo_{11}O_{39}]^{5-}$	–	−0.26	0.14

their presence has on the chemical shift of the phosphorus in the anion. No evidence of a peak corresponding to $H_3[PMo_{12}O_{40}]\cdot\sim28H_2O$ was present in any of the spectra. The trend in chemical shift may be related to the ability of the cations to remove electron density from the anion, thereby deshielding the phosphorus, which is in turn related to the cationic charge. This is likely limited by the relative numbers of cations/$[PMo_{12}O_{40}]^{3-}$ ion and their (average) association with the anions, which is lowest for the Al^{3+} salt, perhaps accounting for less deshielding than in the Mg^{2+} salt. However, Black et al. [40] have pointed out that the solid-state isotropic chemical shift of phosphorus may not necessarily reflect the ionicity of a lattice, as it is not solely dictated by the diamagnetic term in the chemical shift tensor.

In the three salts, the presence of several other signals was also apparent, slightly to more positive chemical shifts (higher frequencies) than for the $[PMo_{12}O_{40}]^{3-}$ ion. Small peaks were observed at −3.84 for $Na_3[PMo_{12}O_{40}]\cdot\sim29H_2O$, −3.41 for $Mg_3[PMo_{12}O_{40}]_2\cdot\sim58H_2O$ (see Fig. 2) and two peaks at −3.70 and at −3.79 ppm for $Al[PMo_{12}O_{40}]\cdot\sim29H_2O$. These are all within 0.42 ppm of the $[PMo_{12}O_{40}]^{3-}$ ion, and all have an intensity of <∼10% of the major peak in each case. The phosphopolyoxomolybdate species with a resonance closest to that of $[PMo_{12}O_{40}]^{3-}$ is $[P_2Mo_{18}O_{62}]^{6-}$, as is evident from the data in Table 1 (with a difference of 0.70 ppm to higher frequencies). Similarly, the solid-state ^{31}P resonances of $K_6[P_2Mo_{18}O_{62}]$ and $(NH_4)_6[P_2Mo_{18}O_{62}]$ (both with water and 1,4-dioxane crystallized in their lattices) occur at about −3.4 and −3.3 ppm, respectively [9], also to higher frequencies than those of $K_3[PMo_{12}O_{40}]$ and $(NH_4)_3[PMo_{12}O_{40}]$ ($\delta = -4.71$ and −5.12 ppm, respectively). In these cases the differences are 1.3 and 1.8 ppm, respectively. Given the chemical shift differences between $[PMo_{12}O_{40}]^{3-}$ and the other phosphopolyoxomolybdate species, it seems unlikely that the extra peaks originate from the presence of co-crystallized hydrolysis species. The identity of these extra peaks can be inferred from ^{31}P NMR solution studies, as discussed below.

The freshly crystallized compounds were quite soluble in water and in polar organic solvents such as acetone, acetonitrile, DMSO and DMF. Consequently, the identity of the extra species was investigated for the $Na^+/[PMo_{12}O_{40}]^{3-}$ system by ^{31}P NMR solution studies in mixed d_6-DMSO/water as the solvent. DMSO was chosen as the organic component for the mixed solvent system as it has been established that it stabilizes the presence of the $[PMo_{12}O_{40}]^{3-}$ ion [8]. In order to obtain a full range of (hydrolysed) anions for study, an aqueous solution of nominal composition $Na_3[PMo_{12}O_{40}]$ was prepared as described above, but allowed to sit for over one week to permit the formation of the Dawson species $[P_2Mo_{18}O_{62}]^{6-}$, which forms relatively slowly as noted above. The water was then removed under vacuum in a dessicator containing silica gel, and TGA measurements indicated that the resulting solid had about 14 water molecules per anion (assuming only $[PMo_{12}O_{40}]^{3-}$ is present). Solvent compositions covered the range 0, 5, 7.5, 10, 25, 50, 75 and 100 mol% DMSO. The spectra showed the presence of $[PMo_{12}O_{40}]^{3-}$ as the main anion present for all solvent compositions, along with various amounts of other anions that changed in relative concentration as the composition of the solvent system was varied. The changes in the chemical shifts and relative intensities of all species are shown in Fig. 3 for the above solvent compositions, with chemical shifts shown relative to $[PMo_{12}O_{40}]^{3-}$, which was set at 0 ppm for the purposes of this study. All of the species present in the initial 100 mol% H_2O solvent were identified based on the previous comprehensive studies of the aqueous $H^+/MoO_4^{2-}/HPO_4^{2-}$ system [28].

Significant changes in both chemical shift and speciation occurred up to ∼10 mol% DMSO, with only small changes in chemical shift above this solvent composition. This is evident from the data as presented in Fig. 4. Both the Dawson species $[P_2Mo_{18}O_{62}]^{6-}$ and the lacunary species $[H_2PMo_{11}O_{39}]^{5-}$ showed initial low and high frequency resonance shifts, respectively, relative to $[PMo_{12}O_{40}]^{3-}$, but much greater effects were observed for the anionic species containing nine molybdenum atoms. In particular, α-A-$[PMo_9O_{31}(H_2O)_3]^{3-}$ appeared to be present only over the solvent composition range from 0 to 10 mol% DMSO, while a second species, which is assumed to be α-A-$[PMo_9O_{31}(OH)(H_2O)_2]^{4-}$ based on the similarity of

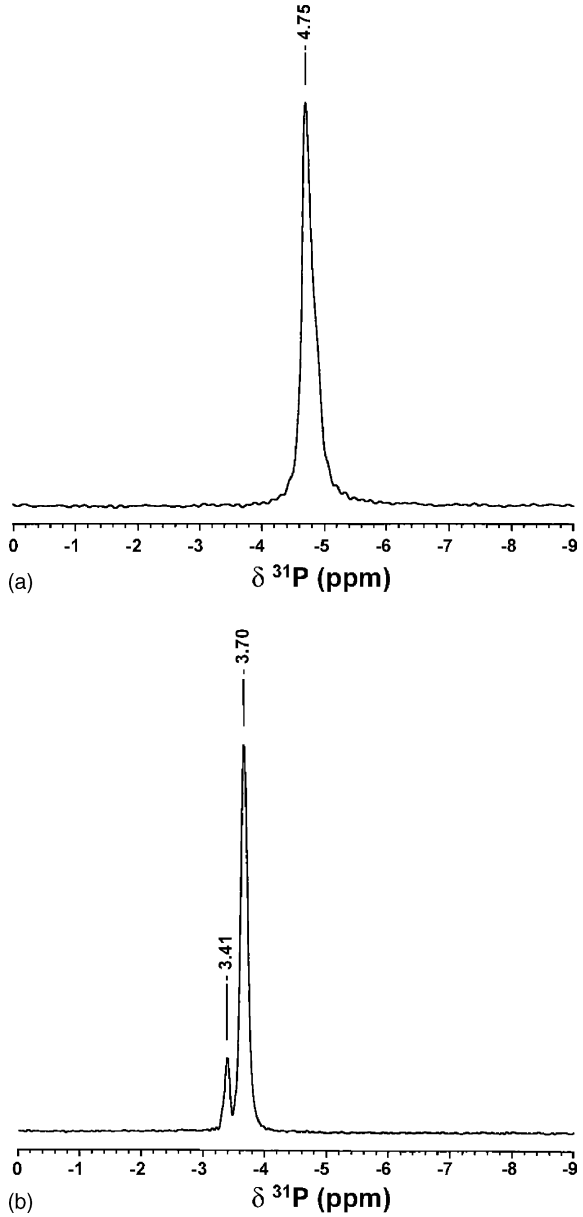

Fig. 2. Solid-state ^{31}P nuclear magnetic resonance spectra of (a) $H_3[PMo_{12}O_{40}]\cdot\sim 28H_2O$, (b) $Mg_3[PMo_{12}O_{40}]_2\cdot\sim 58H_2O$, [$(NH_4)H_2PO_4$, $\delta = 1.00$ ppm]. The peak at -3.41 ppm is a lower hydrate formed during preparation or subsequent handling (<∼10% presence).

its chemical shift to that of α-A-$[PMo_9O_{31}(H_2O)_3]^{3-}$, appeared only above 7.5 mol%. Both species coexisted over the range from 7.5 to 10 mol% DMSO. Despite the fact that the two formulations listed above only differ by a single proton, H^+ exchange is presumably slow enough so that both can be observed on the NMR timescale over this solvent composition range. Such behaviour is not unprecedented. Both $[HSiW_9V_3O_{40}]^{6-}$ and $[SiW_9V_3O_{40}]^{7-}$ coexist in CH_3CN solution as separate species (no H^+ exchange under the reaction conditions) when $[H_3SiW_9V_3O_{40}]^{4-}$ is deprotonated by 3 equivalents of $Bu_4N^+OH^-/CH_3OH$, as shown by ^{51}V and ^{183}W NMR, while four equivalents result in complete deprotonation, although some decomposition of the fully deprotonated species is also evident [41]. The α-B-$[PMo_9O_{34}]^{9-}$ ion (certainly protonated) exhibited a high frequency shift relative to $[PMo_{12}O_{40}]^{3-}$ from 0 to 7.5 mol% DMSO, but disappeared as a species above 7.5 mol% DMSO. This disappearance may perhaps be related to the coexistence of both α-A-$[PMo_9O_{31}(OH)(H_2O)_2]^{4-}$ and α-A-$[PMo_9O_{31}(H_2O)_3]^{3-}$ over the range from 7.5 to 10 mol% DMSO. The species that has been suggested to have a Mo/P ratio of >12 was only observed in 100 mol% H_2O.

Examination of crystallized $Na_3[PMo_{12}O_{40}]\cdot\sim 29H_2O$ by ^{31}P NMR spectroscopy in d_6-DMSO indicated the presence of the major species $[PMo_{12}O_{40}]^{3-}$ at -2.99 ppm (relative to 85% H_3PO_4), in agreement with previously reported data on this ion in DMSO [42], and a second species at -0.23 ppm. This latter resonance is 2.76 ppm to higher frequency than $[PMo_{12}O_{40}]^{3-}$ and from the data in Figs. 3 and 4 therefore corresponds to the lacunary species $[H_2PMo_{11}O_{39}]^{5-}$. This species presumably arises from fast hydrolysis of the $[PMo_{12}O_{40}]^{3-}$ ion by the presence of the original water of crystallization now in solution. Moreover, when the freshly prepared solution was allowed to sit for several days, a new resonance appeared at -1.46 ppm, which can be identified as the nine-molybdenum atom species α-A-$[PMo_9O_{31}(OH)(H_2O)_2]^{3-}$. Thus further slow hydrolysis takes place and must also be caused by the added presence of water which came from the water of crystallization that was contained in the original salt (∼$29H_2O$/Keggin anion). On standing no further hydrolysis was evident.

The ^{31}P NMR data in d_6-DMSO solution for all three species of the type $(M^{n+})_{3/n}[PMo_{12}O_{40}]\cdot\sim 29H_2O$, where $M^{n+} = Na^+$, Mg^{2+} and Al^{3+}, are given in Table 5, along with the data in the solid-state. The presence of $[H_2PMo_{11}O_{39}]^{5-}$ in all of the solution spectra is evident (∼10–20% based on integrated intensities). However, no resonances corresponding to the extra peaks close in chemical shift to the $[PMo_{12}O_{40}]^{3-}$ ion that were observed in the solid-state spectra are observed in solution. It is likely that the extra peaks observed in the solid-state spectra were thus caused by some dehydration of the $(M^{n+})_{3/n}[PMo_{12}O_{40}]\cdot\sim 29H_2O$ species during preparation, or could even result from crystallization of some lower hydrate(s) during the crystallization process. Thermal dehydration from the high-powered ^{1}H decoupling would seem unlikely, as no extra peaks were observed for $H_3[PMo_{12}O_{40}]\cdot\sim 28H_2O$. Thus despite facile loss of water from fully-hydrated species of the type $(M^{n+})_{3/n}[PMo_{12}O_{40}]\cdot\sim 29H_2O$, where $M^{n+} = Na^+$, Mg^{2+} and Al^{3+}, there is no evidence that they contain co-crystallized hydrolysis products, which is in agreement with the IR data presented above. This was also confirmed by the solid-state ^{31}P NMR resonance of the $[HPMo_{11}O_{39}]^{6-}$ ion in $(NH_4)_6[HPMo_{11}O_{39}]$, which was observed at -1.73 ppm. Only a minor difference in chemical shift would be expected as a result of the difference in protonation

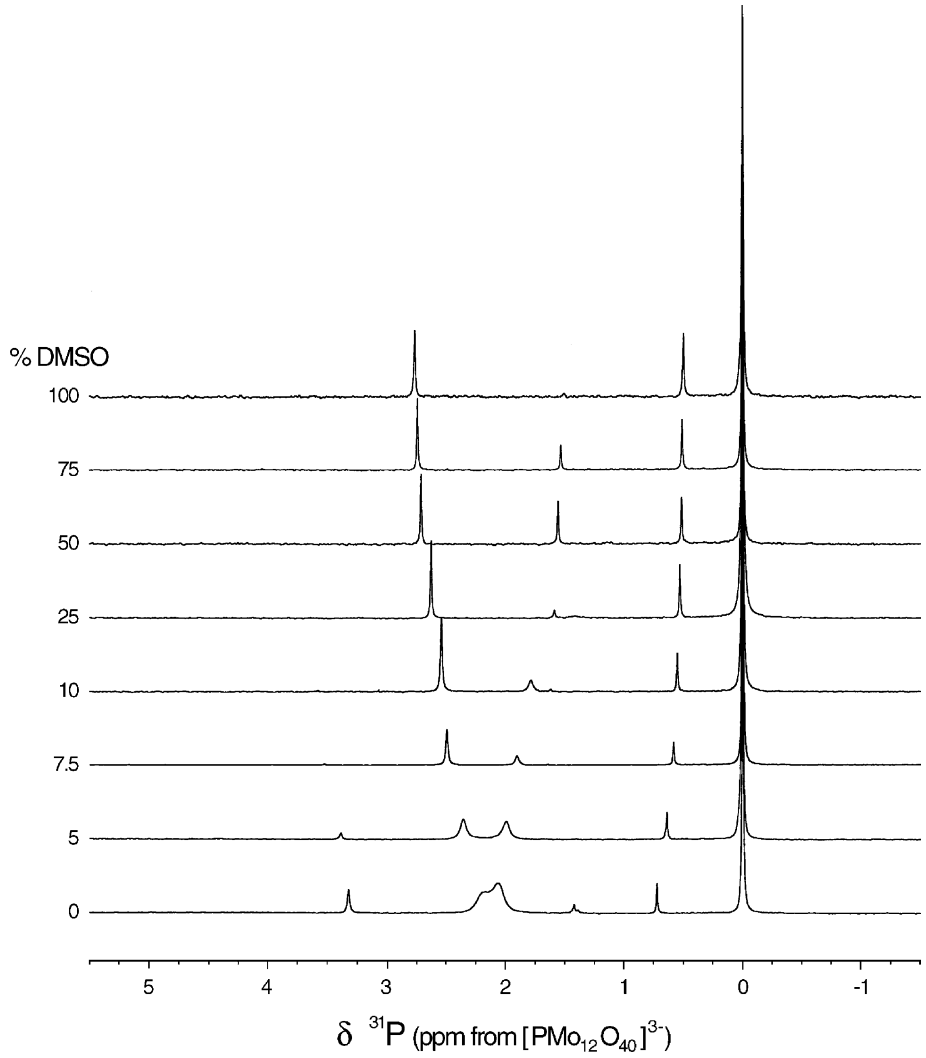

Fig. 3. Solution ^{31}P NMR spectra of the $Na^+/[PMo_{12}O_{40}]^{3-}$ system (with a nominal Na^+:$[PMo_{12}O_{40}]^{3-}$ mole ratio = 3:1) in 0–100 mol% H_2O–DMSO (relative to $\delta = 0$ ppm for the $[PMo_{12}O_{40}]^{3-}$ ion). The changes in chemical shifts of $[P_2Mo_{18}O_{62}]^{6-}$ and $[H_2PMo_{11}O_{39}]^{5-}$ can clearly be seen, and the simultaneous presence of α-A-$[PMo_9O_{31}(H_2O)_3]^{3-}$ and α-A-$[PMo_9O_{31}(OH)(H_2O)_2]^{4-}$ can be observed at 7.5 and 10 mol% H_2O–DMSO.

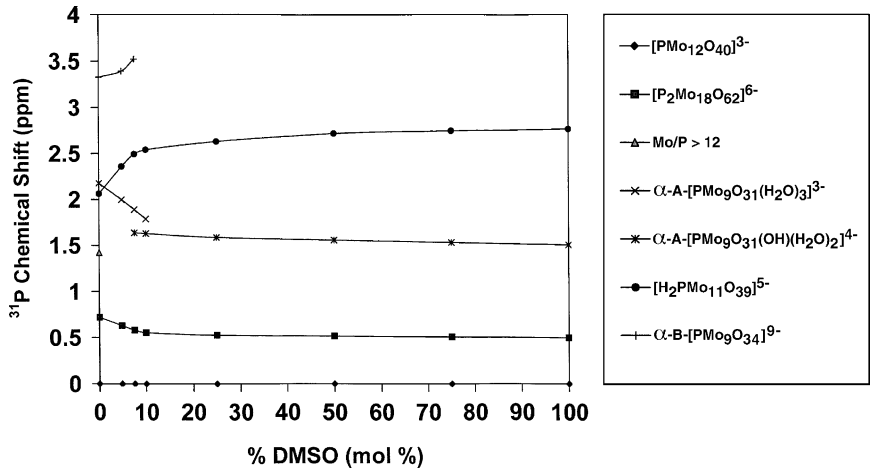

Fig. 4. Relationship between the solution ^{31}P chemical shift and solvent composition (0–100 mol% H_2O–DMSO) for the observed phosphopolyoxomolybdate anions present in the $Na^+/[PMo_{12}O_{40}]^{3-}$ system (relative to $\delta = 0$ ppm for the $[PMo_{12}O_{40}]^{3-}$ ion).

(i.e. $[HPMo_{11}O_{39}]^{6-}$ compared to $[H_2PMo_{11}O_{39}]^{5-}$), but notably the ^{31}P resonance of $(NH_4)_6[HPMo_{11}O_{39}]$ is found at a significantly higher frequency than that for $(NH_4)_3[PMo_{12}O_{40}]$ ($\delta = -5.12$ ppm). The former resonance is broad, with a linewidth at half-height of ~230 Hz, which is much larger than that of the $[PMo_{12}O_{40}]^{3-}$ ion (57 Hz) in the latter. This likely reflects the lowering of local symmetry around the phosphorus in $[HPMo_{11}O_{39}]^{6-}$ and/or several independent anion sites in the unit cell.

Separate studies were also made to see how little $(NH_4)_6[HPMo_{11}O_{39}]$ impurity could be detected in a sample of $(NH_4)_3[PMo_{12}O_{40}]$ by recording the solid-state ^{31}P NMR spectra of 5 and 10 mol% $(NH_4)_6[HPMo_{11}O_{39}]$ in $(NH_4)_3[PMo_{12}O_{40}]$. At 10 mol%, the $(NH_4)_6[HPMo_{11}O_{39}]$ "impurity" could readily be seen, while at 5 mol% the resonance of $(NH_4)_6[HPMo_{11}O_{39}]$ was just noticeable. Based on these studies, therefore, the solid-state ^{31}P NMR spectra of the $(M^{n+})_{3/n}[PMo_{12}O_{40}]\cdot\sim 29H_2O$ compounds, where $M^{n+} = Na^+$, Mg^{2+} and Al^{3+}, show that there would have been less than 5 mol% of any hydrolysis product in the bulk samples.

3.1.5. X-ray powder diffraction studies

All of the crystallized solids were examined by X-ray powder diffraction. The X-ray profile data were fitted by Rietvelt profile analysis using the program RIETICA [26], and were based on a cubic unit cell (space group *Fd*3*m*, $Z = 4$ or 8, depending on the number of formula units in the unit cell), with $a \approx 23.3$ Å. No evidence for other crystalline or amorphous phases was observed. Only Mo, P and the O anion atoms were used in the refinements, and no cations or oxygen atoms from the water molecules of crystallization could be located. The resulting R_{Bragg} values ranged from 18 to 20%. The unit cell data are given in Table 6, along with the data for the hydrated parent acid and previous data on the alkaline earth metal salts [31,32]. The results confirm the previous data, and also show that the same unit cell and structure is obtained when Li^+, Na^+ and Al^{3+} are the ions present in the solutions from which the solids are obtained.

Table 6
Crystallographic unit cell parameters (cubic, *Fd*3*m*) for the hydrated acid and nominal salts of the $[PMo_{12}O_{40}]^{3-}$ ion

Compound	a (observed), Å ($Z = 4$)	a (literature), Å ($Z = 4$)[a,b]
$H_3[PMo_{12}O_{40}]\cdot\sim 29H_2O$	–	23.31 ($Z = 8$) [c,d]
$Mg_3[PMo_{12}O_{40}]_2\cdot\sim 58H_2O$	23.333(2)	23.11
$Ca_3[PMo_{12}O_{40}]_2\cdot\sim 58H_2O$	23.389(3)	23.11
$Sr_3[PMo_{12}O_{40}]_2\cdot\sim 58H_2O$	23.332(3)	23.10
$Ba_3[PMo_{12}O_{40}]_2\cdot\sim 58H_2O$	23.256(8)	23.10
$Li_3[PMo_{12}O_{40}]\cdot\sim 29H_2O$	23.315(3) ($Z = 8$)	–
$Na_3[PMo_{12}O_{40}]\cdot\sim 29H_2O$	23.334(5) ($Z = 8$)	–
$Al[PMo_{12}O_{40}]\cdot\sim 29H_2O$	23.258(3) ($Z = 8$)	–

[a] From [31].
[b] From [32].
[c] Commercial samples.
[d] From [20].

All the solids are isomorphous and isostructural as regards the anion atom locations, and also with the parent acid. Furthermore, the hydrated divalent transition metal salts of the type, $M_3[PMo_{12}O_{40}]_2\cdot 58H_2O$, where $M = Mn^{2+}$, Co^{2+}, Ni^{2+}, Zn^{2+} and Cd^{2+}, have all been reported to have cubic unit cells with $a = 23.10$–23.13 Å [32] and thus the same situation pertains for these compounds.

It should be noted that although no cation or oxygen atoms of the water molecules of crystallization could be located, the cations would only contribute a maximum of 6.8% in the case of Ba^{2+}, down to only 0.52% for Li^+, of the total electron density of the compounds. This is based on an average of $29H_2O$ molecules per $[PMo_{12}O_{40}]^{3-}$ ion for the hydrated solids, as established by the TGA results. In contrast, the contribution from the water molecules of crystallization would vary from 23.9% down to 20.4% for salts containing the above two cations, respectively. All of the cations and water molecules of crystallization would be located in the interanionic voids (channels) between the anions (see below), and would be involved in hydrogen bonding with the anion oxygen atoms. If, as is likely, the cations and water molecules are almost completely disordered down the channels, then the relatively small contribution to the electron density of the former, even in the case of the heaviest ion Ba^{2+}, would make the determination of their crystallographic locations extremely difficult using X-rays. The fact that most of the water molecules of crystallization cannot be crystallographically located is also consistent with their zeolitic-like character, which was noted above.

3.2. Structure of $Ba_3[PMo_{12}O_{40}]_2.(55.3)D_2O$ by Rietveld neutron powder diffraction analysis

In an alternative attempt to locate the cations and water molecules of crystallization in the structure of a soluble $M_3[PMo_{12}O_{40}]_2\cdot\sim 58H_2O$ salt (M = Group 2 metal), neutron powder diffraction studies were conducted on the deuterated compound $Ba_3[PMo_{12}O_{40}]_2\cdot(55.3)D_2O$ at 150 K. Neutron diffraction is used to locate both hydrogen and deuterium atom positions because of their favorable neutron cross sections compared to heavier atoms, while with X-ray diffraction the unfavorable scattering lengths of light atoms, such as hydrogen, make their location extremely difficult. Deuteration was undertaken in order to avoid anomalous scattering from the extensive amount of normal hydrogen in the sample, while low temperatures were used to try to reduce thermal motion and make the cations and water molecules easier to locate. As found for the X-ray studies, the anions were easily located and refined, but even at 150 K most of the D_2O molecules (there are ~220 per unit cell) and none of the Ba^{2+} cations (12 per unit cell) could be found. Several oxygen atoms of the D_2O molecules of crystallization were located and refined, including one of those found by McGarvey et al. [18]. The other oxygen water location found in that study could not be refined, which suggests that the crystallization of the water molecules in the interanionic

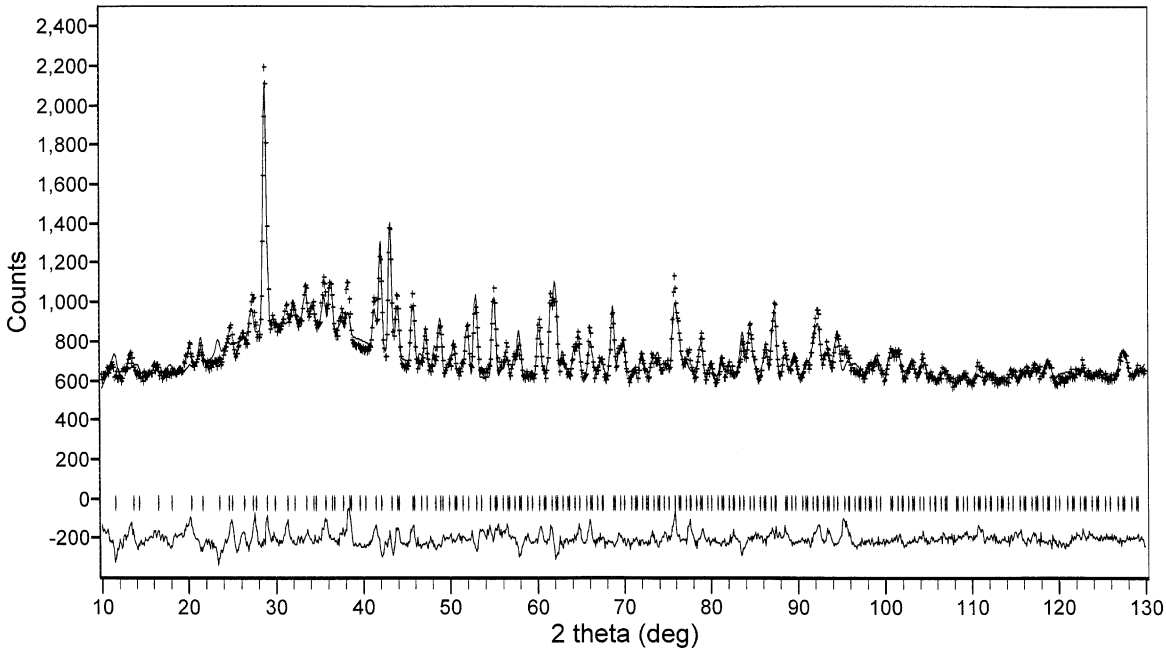

Fig. 5. Fitted neutron powder diffraction pattern and difference pattern for $Ba_3[PMo_{12}O_{40}]_2{\cdot}(55.3)D_2O$ at 150 K. Markers indicate the locations of the Bragg reflections.

voids depends on the crystallization conditions, and can vary from sample to sample. This is consistent with the disorder of water molecules apparent within this structure.

The fitted neutron powder diffraction pattern is shown in Fig. 5, and resulted in a R_{Bragg} of 3.02%. Evident in the pattern is a broad peak located at a 2θ maximum of $\sim 33^\circ$, which arises from the disordered D_2O molecules and Ba^{2+} cations in the unit cell. This is much more apparent in the neutron diffraction study than in the X-ray studies, for the same reasons given above. The presence of this peak indicates extensive disorder within the unit cell and no long-range ordering of the Ba^{2+} cations and water molecules, which is consistent with the ease of loss of water in these types of compounds, as noted previously. Atomic positional parameters are given in Table 7, while selected refinement parameters and bond distances are given in Table 8. These are compared with the data previously obtained from the single-crystal X-ray study [18]. The bond lengths are comparable to those found previously for the $[PMo_{12}O_{40}]^{3-}$ ion [18–20]. A perspective view of the unit cell looking down the 110 direction is given in Fig. 6, and illustrates the channels between the $[PMo_{12}O_{40}]^{3-}$ ions. None of the water molecules of crystallization are shown in this diagram, so as to highlight the channels within the structure. The channels are some 6–11 Å wide based on the interanionic oxygen–oxygen distances of the anions, and these provide enough room for the cations and water molecules of crystallization.

Table 7
Fractional atomic coordinates for $Ba_3[PMo_{12}O_{40}]_2{\cdot}(55.3)D_2O$

Atom	x	y	z	B (Å^2)
Mo	0.0155(3)	0.0155(3)	0.1269(6)	1.7(2)
P	0.1250	0.1250	0.1250	2.6(1.1)
O_a	0.1615(5)	0.1615(5)	0.1615(5)	0.15(8)
O_b	0.1731(4)	0.1731(4)	−0.0042(5)	0.66(26)
O_c	0.0613(3)	0.0613(3)	0.2735(4)	0.45(24)
O_d	0.2846(4)	0.2846(4)	0.1160(7)	1.9(3)
OW(1)	0.377(1)	0.1250	0.1250	4.2(5)
OW(2)	0.351(2)	0.238(2)	0.218(2)	3.7(1.4)[a]
OW(3)	0.619(3)	0.277(3)	0.210(3)	7.3(1.8)[b]

E.S.D.'s in parentheses.
[a] Occupancy = 0.25.
[b] Occupancy = 0.20.

Table 8
Selected structural and refinement parameters for $Ba_3[PMo_{12}O_{40}]_2{\cdot}(55.3)D_2O$

Property	This work, neutron powder diffraction study (temperature = 150 K)	McGarvey et al. [18], X-ray study (temperature = 295 K)
a (Å)	22.941(3)	23.268(1)
V (Å^3)	12074(3)	12597(2)
P–O (Å)	1.45(2)	1.55(1)
Mo–O_a (Å)	2.49(2)	2.42(2)
Mo–O_b (Å)	1.87(1)	1.90(1)
Mo–O_c (Å)	1.98(1)	1.91(1)
Mo–O_d (Å)	1.64(2)	1.69(1)
Mo···Mo (Å)	3.49(2), 3.61(2)	3.40(2)
R_{Bragg} (%)	3.02	–[a]
R_p (%)	3.42	–
R_{wp} (%)	4.41	–
χ^2	6.32	–

[a] No agreement indexes were quoted in reference [18].

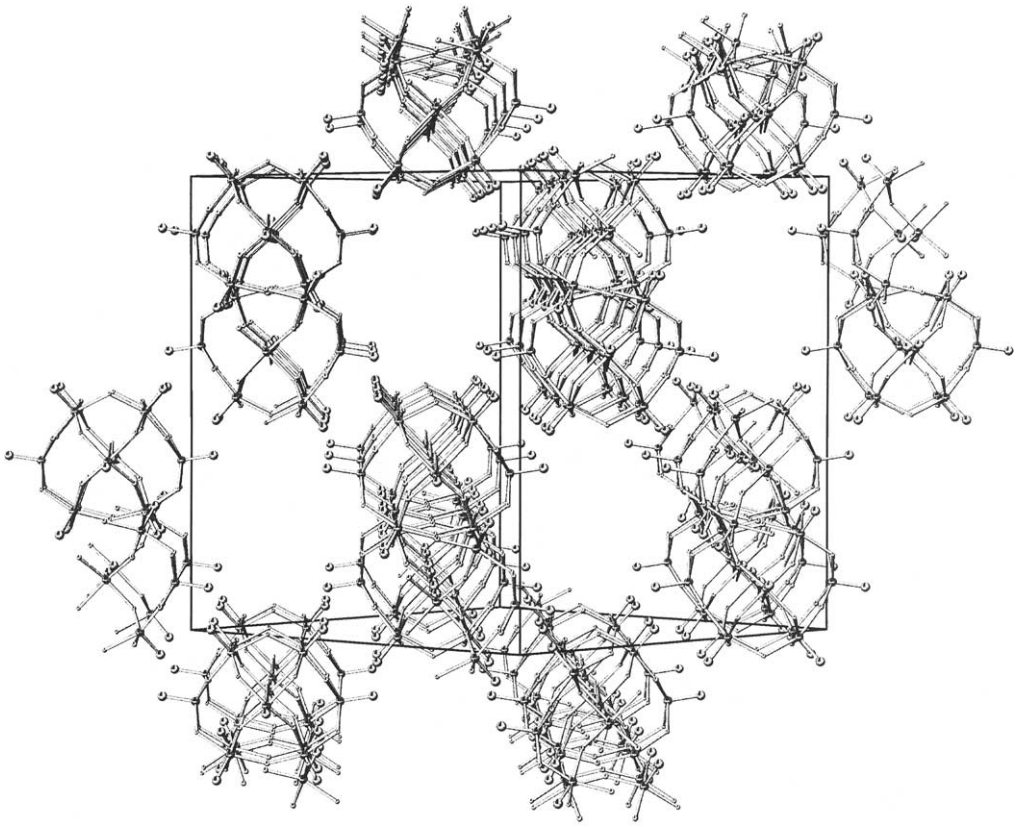

Fig. 6. Unit cell diagram for $Ba_3[PMo_{12}O_{40}]_2{\cdot}(55.3)D_2O$ at 150 K, looking down the 1 1 0 direction (the water of crystallization is not included) to illustrate the channels occupied by the cations and water molecules.

4. Conclusions

The above studies have established the presence of the $[PMo_{12}O_{40}]^{3-}$ ion in the crystallized solids, and chemical analysis has demonstrated the presence of the counter cations. The variations in the rates of crystallization of the solids also suggest the influence of the cations, as do the dependences of the TGA/DTA profiles on the cations, as well as both the IR spectra of the dehydrated compounds and the solid-state ^{31}P NMR studies. The X-ray powder diffraction studies on all crystallized solids at room temperature and the neutron powder diffraction study on $Ba_3[PMo_{12}O_{40}]_2{\cdot}(55.3)D_2O$ at 150 K, although unable to locate the cations or most water molecules of crystallization as a result of extensive disorder, provided no evidence for a second (or more) crystalline or amorphous phase. The latter would have been observable if the crystallized materials were mixtures of the parent acid and a simple alkaline earth (or a Group 1 or 13) metal salt (presumably either a phosphopolyoxomolybdate, polyoxomolybdate or simple molybdate), as suggested by McGarvey et al. [17,18]. We conclude that soluble $[PMo_{12}O_{40}]^{3-}$ salts of the Group 1, 2 and 13 metals can be crystallized and isolated, although because of their ready loss of water of crystallization, some level of variation in the latter can occur as is observed for the acid itself.

Acknowledgements

The authors would like to acknowledge Mr. J.-P. Guerbois of U.T.S. for the DTA measurements, Ms. J. Zobec for help in recording the X-ray data and Dr. J. Hook of U.N.S.W. for obtaining the solid-state ^{31}P NMR data. Dr. B. Hunter, of the Bragg Institute, ANSTO, is thanked for his guidance and help in obtaining the neutron powder diffraction data. Ms. E. Silviani would also like to acknowledge the University of Padun, Indonesia (DUE Project) for financial support. The authors would also like to thank the Australian Institute of Nuclear Science and Engineering for providing financial assistance (Award No. 01/139S) to enable work on the structure of $Ba_3[PMo_{12}O_{40}]_2{\cdot}(55.3)D_2O$ to be conducted.

References

[1] M. Akimoto, Y. Tsuchida, K. Sato, E. Echigoya, J. Catal. 72 (1981) 83.
[2] Y. Konishi, K. Sakata, M. Misono, Y. Yoneda, J. Catal. 77 (1982) 169.
[3] M. Misono, Catal. Rev.-Sci. Eng. 29 (1987) 269.
[4] M. Misono, Catal. Rev.-Sci. Eng. 30 (1988) 339.
[5] M. Misono, in: M.T. Pope, A. Muller (Eds.), Polyoxometalates: From Platonic Solids to Anti-Retroviral Activity, Kluwer, Dordrecht, 1994, p. 255.

[6] N. Mizuno, M. Misono, Chem. Rev. 98 (1998) 199.
[7] J. Hu, R. Burns, J. Catal. 195 (2000) 360.
[8] M.T. Pope, Heteropoly and Isopoly Oxometalates, Springer, Berlin, 1983.
[9] J. Hu, R.C. Burns, J.-P. Guerbois, J. Mol. Catal. A: Chem. 152 (2000) 141.
[10] H. Hayashi, J.B. Moffat, J. Catal. 81 (1983) 61.
[11] T. Baba, H. Watanabe, Y. Ono, J. Phys. Chem. 87 (1983) 2406.
[12] Y. Saito, H. Niiyama, J. Catal. 106 (1987) 329.
[13] J.C.A. Boeyens, J. McDougal, J.V.R. Smit, J. Solid State Chem. 18 (1976) 191.
[14] J.B. McMonagle, J.B. Moffat, J. Colloid Interface Sci. 101 (1984) 479.
[15] D.B. Taylor, J.B. McMonagle, J.B. Moffat, J. Colloid Interface Sci. 108 (1985) 278.
[16] G.B. McGarvey, J.B. Moffat, J. Colloid Interface Sci. 125 (1988) 51.
[17] G.B. McGarvey, J.B. Moffat, Catal. Lett. 16 (1992) 173.
[18] G.B. McGarvey, N.J. Taylor, J.B. Moffat, J. Mol. Catal. 80 (1993) 59.
[19] R. Strandberg, Acta Chem. Scand. A 29 (1975) 359.
[20] R. Allmann, Acta Chem. Scand. A 30 (1976) 152.
[21] M. Fournier, R. Massart, C. R. Acad. Sc. Paris, Série C 279 (1974) 875.
[22] C. Rocchiccioli-Deltcheff, R. Thouvenot, J. Chem. Rev. (S) (1977) 46;
C. Rocchiccioli-Deltcheff, R. Thouvenot, J. Chem. Rev. (M) (1977) 549.
[23] D.T. Harris, Quantitative Chemical Analysis, fifth ed., W.H. Freeman and Company, NY, 1999, p. 102.
[24] Standard Methods for the Examination of Water and Wastewater, in: A.E. Eaton, L.S. Clesceri, A.E. Greenberg (Eds.), APHEA, nineteenth ed., 1995, Section 3120B.
[25] USEPA: Office of Solid Waste, Test Methods for Evaluating Solid Waste, Physical/Chemical Methods (Publication SW-846), third ed., 1996, Method 6010B.
[26] B.A. Hunter, RIETICA, A visual Rietveld program, IUCR Commission Powder Diffr. Newslett. 20 (1998) 21.
[27] G.A. Tsigdinos, Ind. Eng. Chem., Prod. Res. Dev. 13 (1974) 267.
[28] L. Pettersson, I. Andersson, L.-O. Öhman, Inorg. Chem. 25 (1986) 4726.
[29] M. Pohl, Y. Lin, T.J.R. Weakley, K. Nomiya, M. Kaneko, H. Weiner, R.G. Finke, Inorg. Chem. 34 (1995) 767.
[30] H. D'Amour, R. Allmann, Z. Anorg, Allgem. Chem. 143 (1976) 1.
[31] A. Ferrari, L. Cavalca, M. Nardelli, Gazz. Chim. Ital. 78 (1948) 551.
[32] A. Ferrari, L. Cavalca, M. Nardelli, Gazz. Chim. Ital. 79 (1949) 61.
[33] V.M. Bondareva, T.V. Andrushkevich, R.I. Maksimovskaya, L.M. Plyasova, A.V. Ziborov, G.S. Litvak, L.G. Detusheva, Kinet. Catal (Eng. Trans.) 35 (1994) 114.
[34] M. Fournier, C. Feumi-Jantou, C. Rabia, G. Hervé, S. Launay, J. Mater. Chem. 2 (1992) 971.
[35] M. Eigen, Pure Appl. Chem. 6 (1963) 105.
[36] K. Eguchi, N. Yamazoe, T. Seiyama, Nippon Kagaku Kaishi (1981) 336.
[37] C. Rocchiccioli-Deltcheff, R. Thouvenot, R. Franck, Spectrochim. Acta, Part A 32A (1976) 587.
[38] C. Rocchiccioli-Deltcheff, M. Fournier, R. Franck, R. Thouvenot, Inorg. Chem. 22 (1983) 207.
[39] J. Hu, Ph.D. Thesis, University of Newcastle, 1999.
[40] J.R. Black, N.J. Clayden, L. Griffiths, J.D. Scott, J. Chem. Soc., Dalton Trans. (1984) 2765.
[41] R.G. Finke, B. Rapko, R.J. Saxon, P.J. Domaille, J. Am. Chem. Soc. 108 (1986) 2947.
[42] R. Massart, R. Contant, J.M. Fruchart, M. Ciabrini, M. Fournier, Inorg. Chem. 16 (1977) 2916.